

Weakening and Shifting of the Saharan Heat Low Circulation During Wet Years of the West African Monsoon

Ravi Shekhar (ravi.shekhar@yale.edu)
William R. Boos
Yale University, New Haven, Connecticut

September 2016

Abstract

The correlation between increased West African monsoon rainfall and anomalously low surface pressure over the Sahara is well established in observations and global climate models, and has been interpreted as a strengthening of the Saharan Heat Low (SHL) during wet monsoon years. This study uses two atmospheric reanalysis datasets to examine interannual variability of Sahel rainfall and the shallow Saharan Heat Low circulation, which consists of the near surface SHL and the Saharan High in the lower mid-troposphere. During wet Sahel years, the SHL circulation shifts poleward, producing a drop in low-level geopotential height and surface pressure over the Sahara. Statistically removing the effect of the poleward shift from the low-level geopotential eliminates significant correlations between this geopotential and Sahel precipitation. As the SHL circulation shifts poleward, its mid-tropospheric divergent outflow decreases, indicating a weakening of its overturning mass flux. The poleward shift and weakening of the SHL circulation during wet Sahel years is reproduced in an idealized, zonally periodic model of West Africa; a wide range of imposed sea surface temperature and land surface albedo perturbations in this model produce a much larger range of variations in the SHL that nevertheless have similar quantitative associations with Sahel rainfall as in the reanalyses. These results disprove the idea that enhanced Sahel rainfall is caused by strengthening of the SHL overturning. Instead, a stronger SHL circu-

lation inhibits Sahel rainfall, or some other forcing causes both an increase in Sahel rainfall and a weakening of the SHL circulation.

1 Introduction

Over the twentieth century, large interannual and interdecadal variations in precipitation were observed in the African Sahel, producing occasional floods and sustained droughts. A variety of studies examined the cause of these variations (e.g. Charney et al., 1975; Folland et al., 1986; Eltahir and Gong, 1996; Nicholson and Grist, 2001), but a robust explanation was not established until Giannini et al. (2003) showed that much of the observed variability could be reproduced if observed global SSTs were used to drive a global climate model, implicating SST as the primary cause of historical Sahel precipitation changes.

While it is now generally agreed that SST drives interdecadal variations in Sahel precipitation (e.g. Nicholson, 2013), the Sahara desert is also known to be associated with Sahel variability on a range of time scales. Haarsma et al. (2005) found a correlation on interannual time scales between increased Sahel rainfall and decreased mean sea level pressure over the Sahara. They argued that variations in the mean sea level pressure gradient between the Sahara and its surroundings cause variations in low-level convergence of mass and moisture, and thus in rainfall, over the Sahel. They furthermore argued that the mean sea level pressure gradient is set by

the land-ocean temperature contrast, which can then be viewed as a fundamental driver of Sahel rainfall. In contrast, Biasutti et al. (2009) found that land-ocean temperature contrast is poorly correlated with Sahel precipitation at interannual time scales in CMIP3 models. They argued that while variations in Sahel rainfall are indeed caused by variations in the strength of the low-level circulation over the Sahara, the meridional gradient of 925 hPa geopotential height is a better indicator of the strength of the Saharan Heat Low (SHL; e.g. R acz and Smith, 1999), which is a dry, shallow overturning circulation centered in the Sahara desert. At interannual time scales, Biasutti et al. (2009) found that when the 925 hPa geopotential was anomalously low over the Sahara, the SHL was strong and there was greater rainfall over the Sahel. They also showed that 925 hPa geopotential height anomalies over the Sahara led Sahel rainfall anomalies by a month, suggesting that the SHL causes, and is not just correlated with, Sahel rainfall variability.

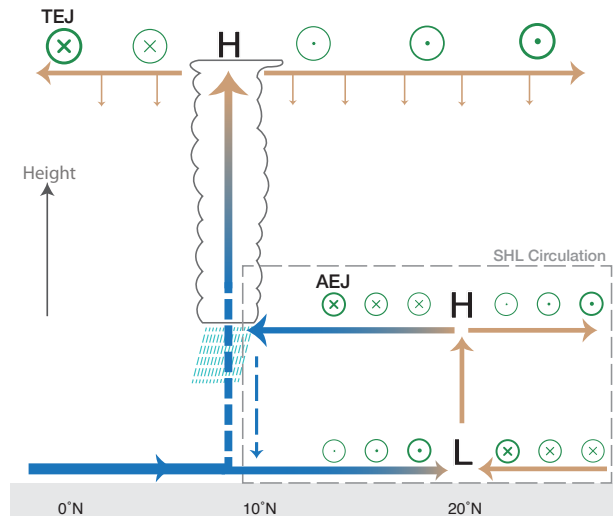


Figure 1: The near-surface Saharan Heat Low cyclone is indicated by an “L” at 20°N , the mid-level Saharan High anticyclone is indicated by an “H” at 20°N , and the combination of these is collectively referred to as the SHL circulation. The divergent component of the SHL circulation, indicated by arrows in the dashed box, is the Saharan overturning. The mid-level African Easterly Jet (AEJ), upper-level Tropical Easterly Jet (TEJ), and upper level anticyclone in the ITCZ are also shown.

Mechanistically, both Haarsma et al. (2005) and Biasutti et al. (2009) argue that an anomalously strong near-surface SHL creates increased low-level mass convergence over the Sahara, and this enhanced circulation causes more moisture convergence and rainfall over the Sahel. Other studies have echoed this view, including Lavaysse et al. (2009), who make the additional point that the near-surface SHL plays a crucial role in West African monsoon onset through its low level cyclonic circulation. Lavaysse

et al. (2010a) show enhanced deep convection over the Sahel during strong phases of the SHL, where a strong SHL is identified by LLAT being anomalously high. During weak phases, when the Saharan LLAT is anomalously low, deep convection over the Sahel is suppressed. However, in another study from the same year, Lavaysse et al. (2010b) show that when the SHL circulation interacts with the midlatitudes on intraseasonal timescales, the opposite sign of correlation can be observed, with low LLAT over the Sahara corresponding to increased deep convection over the Sahel.

The picture becomes even less clear when one considers studies describing the influence of the mid-tropospheric Saharan High on Sahel precipitation. In a pair of companion studies, Peyrillé et al. (2007) and Peyrillé and Lafore (2007) used an idealized, zonally symmetric model of the West African monsoon to examine the influence on Sahel rainfall of the large-scale temperature and moisture advection produced by the SHL circulation. They used an atmospheric reanalysis to show that the SHL circulation produces near-surface cooling and moistening over the Sahel and Sahara, and warming and drying in the lower mid-troposphere (around 700 hPa). Furthermore, when they imposed these low- and mid-level advective tendencies individually in their idealized model, they found that the low-level cooling and moistening caused increased Sahel rainfall, while the mid-level warming and drying caused decreased Sahel rainfall. The effect of the mid-level warming and drying dominated, so that temperature and moisture advection in the SHL circulation has a net inhibitory effect on Sahel rainfall. This is consistent with the demonstrated sensitivity of precipitating convection to drying of the free troposphere above the boundary layer (Derbyshire et al., 2004; Holloway and Neelin, 2009; Sobel and Schneider, 2009), but would seem to contradict the idea that a stronger near-surface SHL would cause an increase in Sahel rainfall (e.g. Haarsma et al., 2005; Biasutti et al., 2009), unless the near-surface SHL does not strengthen with the Saharan overturning circulation.

In addition to the correlation between Sahel precipitation and near-surface geopotential, there is an

association of precipitation with changes in winds as well. The low level monsoon westerlies have a maximum at the surface during dry years but form a jet at 850 hPa during wet years (Grist and Nicholson, 2001). The African easterly jet (AEJ), in balance with the strong thermal contrasts between the Sahel and Sahara and maintained by both the deep and shallow circulations (Thorncroft and Blackburn, 1999), exhibits a statistically significant northward shift and weakening during wet Sahel years (Hsieh and Cook, 2005; Dezfuli and Nicholson, 2011). The upper-level tropical easterly jet (TEJ) is also strongly linked to interannual variability over the Sahel, with a significant strengthening during wet years (Nicholson and Grist, 2001; Dezfuli and Nicholson, 2011). There does not seem to be a clear consensus on reasons behind the changes in the AEJ and TEJ, but current understanding is reviewed in Nicholson (2013).

To the best of our knowledge, the observed association of interannual variations in Sahel rainfall with the whole SHL circulation has not been examined. It might seem reasonable to assume that the Saharan overturning circulation would strengthen as the near-surface SHL strengthens, but given the dominant effect of the mid-level warming and drying on Sahel rainfall suggested by an idealized study (Peyrillé and Lafore, 2007), this would be inconsistent with observations of a strengthening of the near-surface SHL during rainy Sahel years. Perhaps low-level cooling and moistening by the SHL circulation has a larger influence on Sahel precipitation in the real world than in the idealized model of Peyrillé and Lafore (2007), similar to suggestions for the role of these low-level tendencies in the observed seasonal northward migration of West African rainfall (e.g. Hagos and Cook, 2007; Thorncroft et al., 2011; Peyrillé et al., 2016). Or perhaps the SHL circulation does not strengthen as the near-surface SHL strengthens. Here we seek to resolve these questions by examining the association of Sahel rainfall with the three-dimensional SHL circulation at interannual timescales in two atmospheric reanalyses and an idealized model.

The next section of this paper describes our data sources and analysis methods. Section 3 discusses

the climatology and basic features of the West African monsoon and SHL circulation. Section 4 examines how the horizontal structure of the near-surface SHL and the Saharan High covary with Sahel precipitation, and is followed by a section detailing the vertical structure of the circulation changes, with emphasis on the divergent component of the flow. Section 7 compares all of these observationally based results with output from an idealized β -plane model. We close with a discussion of implications and caveats in section 8.

2 Methods

We obtain winds, geopotential height, temperature, and humidity from the ERA-Interim reanalysis (Dee et al., 2011), which is produced by the European Centre for Medium-Range Weather Forecasts (ECMWF) and is used here for 1979-2015. ERA-Interim is a third generation reanalysis with data assimilation based on 12-hourly four dimensional variational analysis (4D-Var). The dynamics are calculated on a T255 (approximately 80 km) global grid, with 60 vertical levels from the surface to 0.1 hPa. We also use NASA’s Modern-Era Retrospective analysis for Research and Applications, Version 2 (MERRA2; Gelaro, R. and co-authors, 2016 in preparation), which is a third generation reanalysis produced on a $0.5^\circ \times 0.625^\circ$ cubed-sphere grid with 72 vertical levels from the surface to 0.1 hPa. MERRA2 is not available for 1979, so here we use 1980-2015. All climatologies and regressions shown here use ERA-Interim data unless MERRA2 is explicitly indicated.

The Global Precipitation Climatology Project (GPCP) dataset (Adler et al., 2003), which is a combination of land rain gauge and satellite-based precipitation measurements, is used as the primary precipitation dataset for this study. The Global Precipitation Climatology Centre (GPCC, Schneider et al., 2014) dataset, based on corrected gridded rain gauge data, was also examined and found to produce no substantial changes in the conclusions of this study. All data was obtained at monthly mean resolution.

When we take limited zonal averages, we do so

over 10°W to 25°E , a region that encompasses most of northern hemisphere Africa but excludes coasts and the Arabian Desert. Within these bounds, the latitudes of 10°N to 20°N are defined as the Sahel, and 20°N to 30°N as the Sahara, with both regions delineated with boxes in Fig. 2a. The results in this study are not sensitive to the longitudinal bounds of the region chosen for the Sahara and Sahel, as the correlation of local precipitation with Sahel-averaged precipitation consists of a pattern that extends zonally across Africa (Fig. 2c).

For the idealized model portion of this study, we analyzed the same integrations presented in Shekhar and Boos (2016). These used the Weather Research and Forecasting (WRF) model, version 3.3 (Skamarock et al., 2008), modified to run on an equatorial β -plane in a meridional channel at 15 km resolution with 41 vertical levels. The domain was $20^\circ \times 140^\circ$ in the zonal and meridional directions, respectively, with periodic boundary conditions in the zonal direction and closed boundary conditions in the meridional direction. A continent was prescribed from 5°N to 32°N , divided into a grassland from 5°N – 12°N and a desert from 12°N – 32°N , with interactive surface temperature but prescribed soil moisture and other properties from the WRF land surface database. The remainder of the domain was ocean with a prescribed idealized SST distribution representative of that observed during boreal summer near Africa. Perpetual July 15 insolation was imposed, with the diurnal cycle retained. A total of thirteen model integrations were performed for one model year after a three month spinup, yielding the same amount of output for each integration as four three-month summer seasons. One integration was chosen as the control, and others were forced by modifications of the specified desert surface albedo, the prescribed SST, or both. These form an ensemble of integrations in which the monsoon precipitation varies in response to the SST and surface albedo forcings. These integrations were documented more thoroughly in Shekhar and Boos (2016), where they were used to examine energy-based diagnostics of ITCZ location.

Statistical analyses were performed using Python

programming language packages Iris (U.K. Met Office, 2015), Seaborn (Botvinnik et al., 2016), and Statsmodels (Seabold and Perktold, 2010). For linear regressions, we test for a nonzero slope using a two-sided Student’s t test at the $p < 0.05$ level. For some linear regressions, we also obtain a 95% confidence interval for the slope using a bootstrapping technique on the joint probability distribution of slope and intercept, as given in the Seaborn package. We tested the sensitivity of linear regressions to outliers using the robust regression (e.g. Rousseeuw and Leroy, 2005) feature of the Statsmodels package, and although certain confidence intervals narrow and shift slightly, no substantial qualitative differences were obtained.

3 Review of prior results on the Sahel-SHL connection

To set the stage for our study, we discuss some well-known features of the West African Monsoon and SHL circulation, most of which were reviewed by Nicholson (2013). The monsoon exists in two relevant phases, a coastal phase, in which peak precipitation lies at the coast of the Gulf of Guinea at 5°N , and a continental phase, with peak precipitation near 10°N . The transition from the coastal to the continental phase is called monsoon onset and climatologically occurs around June 20. Over the region we choose as the Sahel ($10^\circ\text{--}20^\circ\text{N}$, $10^\circ\text{W--}25^\circ\text{E}$) the months of June and September have roughly equal amounts of precipitation (not shown), so we choose June-September (JJAS) as our boreal summer monsoon season. During this period, abundant precipitation over land in the monsoon’s continental phase is clearly visible (Fig. 2a). The climatological mean JJAS precipitation averaged over the Sahel is 2.9 mm day^{-1} .

The time series of JJAS precipitation averaged over the Sahel (Fig. 2b, hereafter referred to as “Sahel precipitation”) is in good agreement with similar time series in other studies (Nicholson, 2005; Nicholson et al., 2011). It has an interannual standard deviation of 0.37 mm day^{-1} , indicating that there is about a 1 mm day^{-1} difference between

fairly wet and fairly dry years in the Sahel. Over the reanalysis period of 1979-2015, Sahel precipitation lacks statistically significant interannual autocorrelations (not shown), distinguishing variability in this more recent period from the persistent interdecadal droughts that characterized parts of the twentieth century and that were largely attributed to global variations in SST (Giannini et al., 2003). Losada et al. (2012) noted the non-stationarity of the relationship between Sahel precipitation and SST in the different ocean basins over the twentieth century, and showed a marked transition in SST dependence in the 1970s, with a largely stationary regime of SST dependence since then. In our post-1970s period, precipitation mostly exhibits a “monopole” spatial pattern (Fig. 2c), with single-signed precipitation anomalies extending from the Gulf of Guinea across the Sahel. This is in contrast to meridional “dipole” patterns of precipitation anomalies observed during the 1920s-1970s (Fig. 14 of Nicholson, 2013). This has implications for the generality of our results, which we discuss further in section 8.

Positive anomalies of Sahel rainfall are accompanied by negative anomalies of geopotential height over the Sahara, as shown by Biasutti et al. (2009) and by our regression of ΔZ_{925} on Sahel precipitation (Fig. 2d). We use ΔZ to represent the difference between local geopotential height and the tropical-mean ($30^\circ\text{S--}30^\circ\text{N}$) geopotential height, $\Delta Z = Z - [Z]_{\text{global tropics}}$. A regression of mean sea level pressure on Sahel rainfall yields a similar pattern (not shown). Previous studies interpreted these patterns of ΔZ_{925} and mean sea level pressure as indicative of a strengthening of the SHL (Haarsma et al., 2005; Biasutti et al., 2009). But the near-surface SHL stretches zonally across northern Africa and is centered around 20°N while the decrease in ΔZ_{925} is confined to the northern and western sides of this climatological trough. Since a strengthening of the near-surface SHL would consist of negative anomalies of ΔZ_{925} centered over the climatological minimum ΔZ_{925} , this would seem to indicate that the near-surface SHL is expanding northward and westward rather than simply strengthening. Much of the northward expansion occurs over northeastern

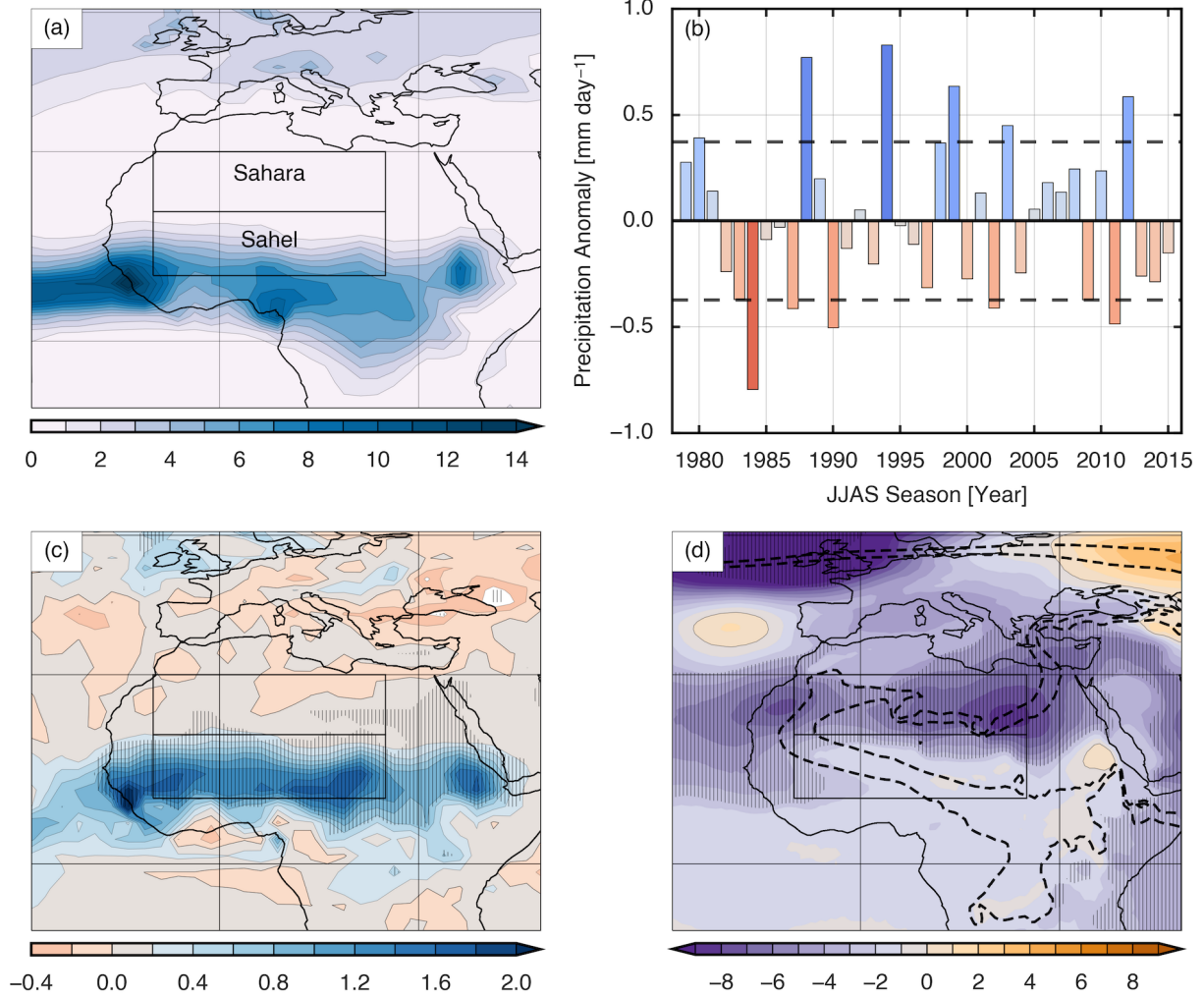


Figure 2: (a) June-September precipitation climatology based on GPCP data, with Sahel and Sahara boxes indicated. Units mm day⁻¹ (b) Interannual time series of precipitation over the Sahel box derived from GPCP data, with ± 1 standard deviation bounds are indicated by dashed lines. (c) Regression slope of local GPCP precipitation onto Sahel area averaged precipitation in mm day⁻¹ per mm day⁻¹. (d) Regression slope of ΔZ_{925} (m mm⁻¹ day; colors) and climatological ΔZ_{925} -10 m and -20 m (contours black dashed). Statistically significant regression slopes ($p < 0.05$) are hatched.

Africa, consistent with the patterns in anomalous ΔZ_{925} and mean sea level pressure seen in Biasutti et al. (2009) and Haarsma et al. (2005).

The near-surface SHL is part of the three-dimensional SHL circulation, as mentioned in the introduction. The ascending branch of the overturning component of this circulation is strongest at around 20°N in the climatological mean (Fig. 3a). Low level mass convergence occurs between the surface and 800 hPa, with peak convergence at 925 hPa associated with the near-surface SHL. Divergence occurs in the 800–550 hPa layer, with peak divergence at 700 hPa associated with the Saharan High. The 925 hPa and 700 hPa levels are taken as representative of the near-surface SHL and the Saharan High, respectively, in the next two sections. Deep ascent in the ITCZ is located much further south, around 8°N . There is weak time-mean divergence and subsidence in the near-surface layer around 10°N in the precipitating region, a likely signal of strong time-mean subsidence and sporadic ascent due to precipitation. The near-surface zonal and meridional winds change sign at 20°N (Fig. 3b), a well-known feature called the Inter-Tropical discontinuity (ITD). Around 700 hPa, there is a peak in the equatorward flow as air travels in the shallow Saharan overturning circulation toward the ITCZ in the time mean. The African Easterly Jet (AEJ; e.g. Thorncroft and Blackburn, 1999) exists in thermal wind balance around 600 hPa and 14°N . At upper levels, the tropical easterly jet, meridional flow in the upper branch of the Hadley circulation, and the midlatitude jet stream are also visible. In the next two sections, we examine how the horizontal and vertical structure of the entire SHL circulation covaries with Sahel precipitation.

4 Horizontal structure of SHL circulation changes

Since the geopotential height and divergent wind together provide a nearly complete depiction of the horizontal circulation, we start by examining the horizontal structure of geopotential and divergent wind variations at 925 and 700 hPa. Fig. 4a shows the 925 hPa climatological trough extending

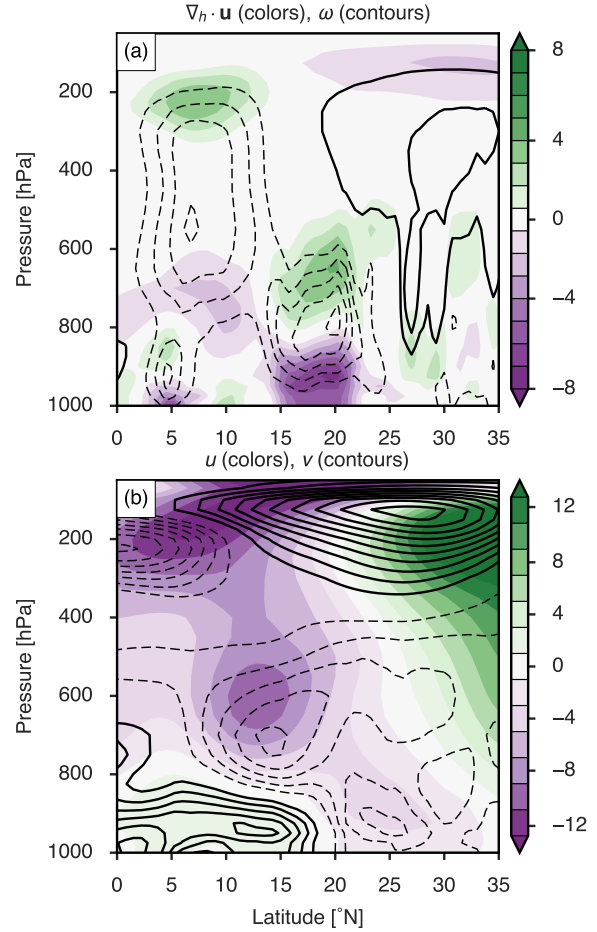


Figure 3: Climatological JJAS time and zonal mean (a) Divergence (colors; 10^{-6} s^{-1}) and pressure velocity ω (contours every 0.5 hPa hr^{-1}). (b) Zonal wind u (colors) and meridional wind v (contours every m s^{-1}). Zero contours are omitted, and negative contours are dashed.

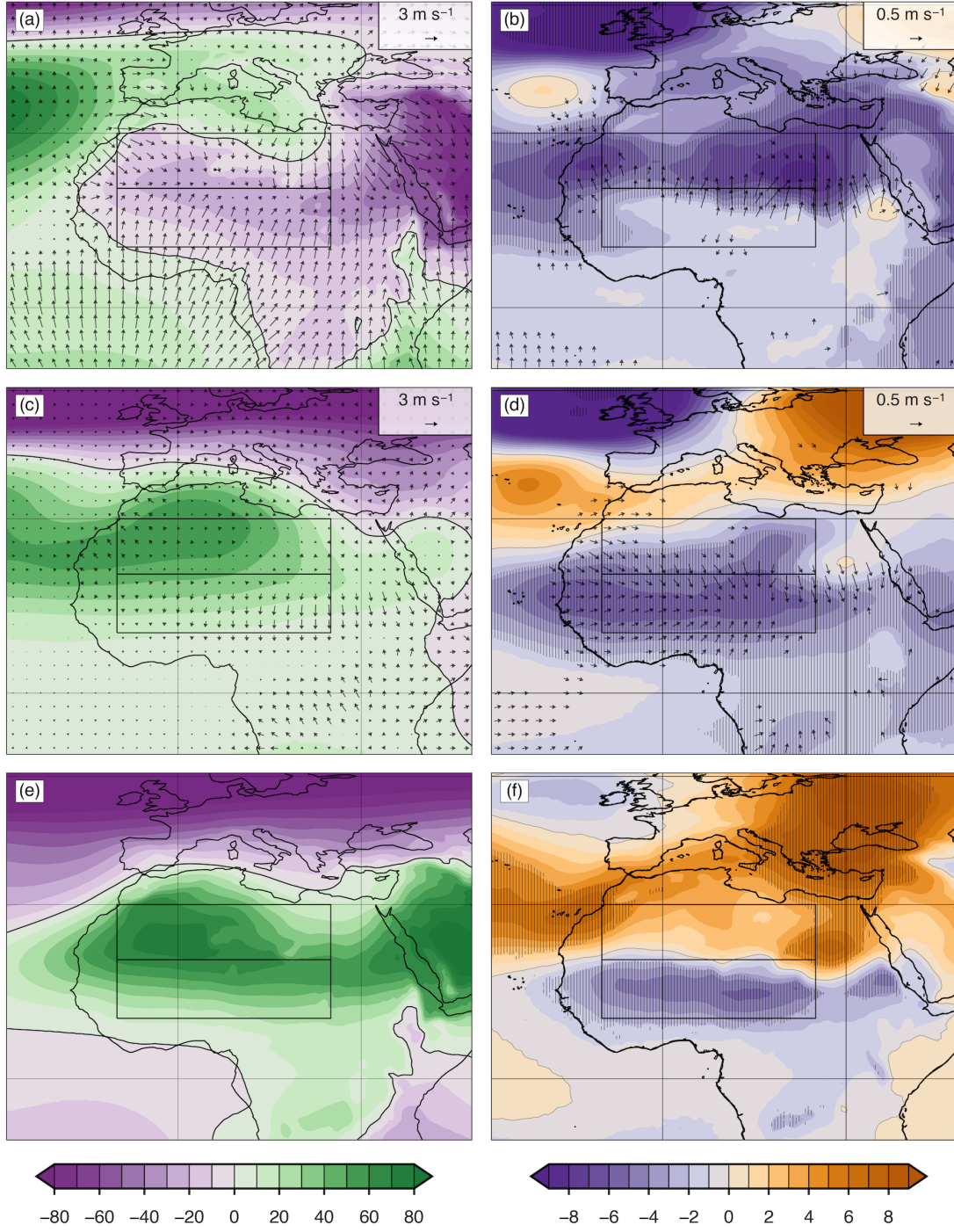


Figure 4: ERA-Interim. (a, c, e) Colors show climatological JJAS ΔZ_{925} , ΔZ_{700} , and LLAT respectively in units of m. Arrows show the divergent component of the wind \mathbf{u}_χ for the same 925 and 700 hPa levels respectively. (b, d, f) Colors show the regression slope of ΔZ_{925} , ΔZ_{700} , and LLAT onto Sahel precipitation respectively ($\text{m mm}^{-1} \text{ day}$), with hatched regions indicating statistical significance. Divergent wind regression slope for same 925 and 700 hPa levels respectively shown in arrows, with only regions where u_χ or v_χ is statistically significant and $|\mathbf{u}_\chi| > 0.1 \text{ m s}^{-1} \text{ mm}^{-1} \text{ day}$ are drawn. Constant tropical climatological value of 2360 m subtracted from all LLAT fields.

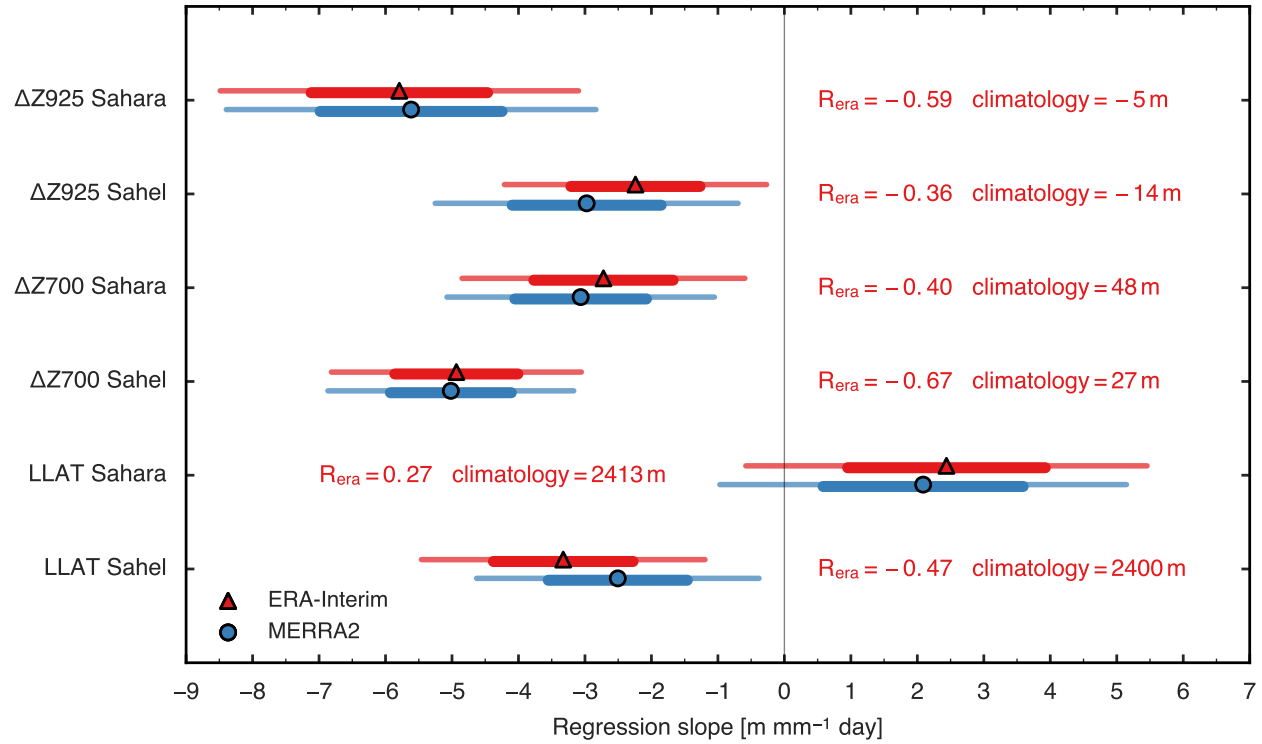


Figure 5: 68% (thick) and 95% (thin) confidence intervals for the slope of the regression in ERA-Interim and MERRA-2 reanalyses. Slopes shown for area averaged height and LLAT regressed onto Sahel precipitation. Critical R values with $n - 2 = 34$ degrees of freedom are 0.329, 0.423, and 0.525 at the 0.05, 0.01, and 0.001 levels.

across northern Africa during JJAS around 20°N; this is accompanied by a cyclonic geostrophic circulation around the trough. Winds converge into the trough around 20°N at the ITD, and cross-equatorial southerly flow in the low-level branch of the Hadley cell is also visible over the Gulf of Guinea. When regressed on Sahel precipitation, we see a spatially heterogeneous but nearly single-signed decrease in ΔZ_{925} (Fig. 4b) north of 20°N over Africa, Europe, and parts of the Atlantic and Indian oceans. The climatological meridional ΔZ_{925} gradient weakens at the southern boundary of the Sahel: although the changes in ΔZ_{925} are not statistically significant there, the anomalous northerly divergent flow during wet years is statistically significant and indicates a weakening of the ageostrophic northward monsoon flow into the Sahel at that level. At the northern boundary of the Sahel, anomalous southerly wind flows across the climatological ITD, into the stronger low in the Sahara. Effectively, this moves the ITD and SHL poleward during wet years. Part of this shift involves a weakening of 925 hPa convergence over the Sahel during wet years; we show in the next section that this can occur because of compensating convergence in the lower mid-troposphere.

Fig. 4c shows the horizontal structure of the climatological mean Saharan High, with gradients in ΔZ_{700} in geostrophic balance with an anticyclone over most of the Saharan region. There is a substantial zonal gradient in ΔZ_{700} over the central and eastern Sahara, and a sharp meridional gradient over the Sahel in balance with the AEJ. The peak in climatological ΔZ_{700} lies poleward and westward of the trough in climatological ΔZ_{925} . Downgradient divergent flow occurs south and northwest of the 700 hPa high, constituting the divergent northerly outflow in the upper branch of the Saharan overturning circulation. The regression of ΔZ_{700} onto Sahel precipitation (Fig. 4d) shows a statistically significant decrease centered in the Sahel that extends over most of northern hemisphere Africa, implying a strong anomalous cyclonic circulation over the whole region during wet years. At 700 hPa, the anomalous divergent wind converges into the center of the anomalous low, around 15°N in the eastern Sa-

hel.

We expect the 925 and 700 hPa surfaces to be affected differently by a strengthening of the shallow SHL circulation compared to a strengthening of the deep, precipitating monsoon circulation. A stronger shallow heat-low circulation is expected to consist of a reduction in ΔZ_{925} in the SHL, an increase in ΔZ_{700} in the Saharan High, and an increase in the divergent, overturning circulation that flows along the geopotential gradients at these two levels. In contrast, enhanced precipitation is expected to be accompanied by enhanced ascent in a deep circulation that can be approximated by a first-baroclinic mode; strengthening of such a first-baroclinic mode will include decreases in geopotential height in the entire lower and middle troposphere and increases in geopotential in the upper troposphere [see Neelin and Zeng (2000) for a derivation of the structure of a typical tropical first-baroclinic mode, and Zhang et al. (2008) or Nie et al. (2010) for illustration of how the shallow Saharan overturning coexists with a precipitating first-baroclinic mode structure over West Africa]. The 925 hPa and 700 hPa surfaces are thus expected to have opposite vertical displacements as the SHL intensifies, while those two surfaces are both expected to move downward as the deep, precipitating circulation strengthens. Fig. 4 (panels b and d) shows that the 700 and 900 hPa surfaces both move downward during wet Sahel years, providing no evidence for a strengthening of the shallow SHL circulation. Furthermore, when geopotential heights are averaged over our Sahel and Sahara boxes, the negative anomalies in ΔZ_{925} and ΔZ_{700} during wet years are found to be statistically significant in both regions (Fig. 5). Thus, geopotential variations at 925 and 700 hPa are inconsistent with the hypothesis that the SHL circulation strengthens during wet Sahel years.

These changes in structure can also be viewed in terms of the thickness of the lower troposphere, but one must remember that LLAT will increase during a strengthening of the shallow heat low circulation and during a strengthening of the deep precipitating circulation. The LLAT climatology (Fig. 4e) shows a maximum over the western Sahara, with rel-

atively high LLAT extending east along the the 20°N line, approximately following the ITD. The regression of LLAT onto Sahel precipitation (Fig. 4f) generally shows a statistically weak increase in LLAT on the poleward side of the climatological LLAT maximum (over the Sahara), and a statistically significant decrease on the equatorward side of this maximum (over the Sahel). While all parts do not achieve statistical significance, especially over the Sahara, the general structure of a meridional dipole without large zonal variations is consistent with the meridional shift we suggested earlier based on the changes in $\Delta Z925$. The lack of zonal variation is important, as it does not show an anomalous thickening of the lower troposphere in the Western Sahara, where the LLAT is climatologically highest. If the SHL circulation was strengthening, we would have expected increased LLAT at its climatological maximum. There are also substantial increases in LLAT over eastern Europe, the Mediterranean, and the Atlantic which might indicate interactions with the midlatitudes, perhaps through mechanisms proposed by Vizu and Cook (2009) and Lavaysse et al. (2010b). Here we simply note that these patterns signify an expansion of the SHL circulation toward those regions.

We now return to examination of our regressions of area-averaged geopotential on Sahel precipitation (Fig. 5). These quantitatively reproduce the result from Biasutti et al. (2009) of decreased Sahara $\Delta Z925$ during wet years, with the ERA-Interim results being quantitatively indistinguishable from the MERRA2 results. We also see decreased $\Delta Z925$ over the Sahel, and an inspection of the climatological values (Fig. 5) indicate that the meridional gradient of $\Delta Z925$ between the Sahara and Sahel flattens during wet years. The Sahel LLAT decreases as a consequence of $\Delta Z925$ decreasing less than $\Delta Z700$ during wet years (in this case, removal of the tropical mean has little effect, with variations in $\Delta Z700 - \Delta Z925$ being nearly equal to variations in $Z700 - Z925$). This is inconsistent with the idea that a classic first-baroclinic mode structure intensifies over the Sahel, and we will show in the next section that the vertical profile of the anomalous convergence during

wet years also differs from that of a classic first-baroclinic mode, but still provides no evidence for a strengthening of the SHL during wet years. Over the Sahara, LLAT does increase during wet years, but the confidence interval on the regression slope does not exclude zero (i.e. the slopes of the regressions of $\Delta Z925$ and $\Delta Z700$ are indistinguishable in that region). Furthermore, the horizontal structures discussed above indicate that this increase in LLAT is better viewed as a poleward shift in the SHL circulation rather than a strengthening.

This poleward shift is clearly seen when we regress the latitude of the SHL on Sahel precipitation (Fig. 6a), with the SHL latitude defined as the latitude of minimum $\Delta Z925$ in the limited zonal average (before finding the latitude of the minimum, we use cubic splines to interpolate zonally averaged $\Delta Z925$ to a continuous domain). The SHL latitude exhibits a strong positive correlation with Sahel rainfall. Both reanalyses contain an influential data point in 1984, which was the driest year in the reanalysis period, with an SHL latitude about 1 degree farther south than in all other years. Removing this extreme data point or using robust regression decreases slopes to approximately 0.55 degrees mm^{-1}day , but does not qualitatively change the relationship between SHL and Sahel precipitation. The MERRA2 data exhibit a somewhat bimodal distribution in SHL latitude, for which we do not have an explanation.

As Sahel precipitation covaries with both Sahara $\Delta Z925$ and SHL latitude, we can ask how much of the drop in Sahara $\Delta Z925$ is due to the SHL trough moving into the Sahara, and how well Sahara $\Delta Z925$ correlates with Sahel precipitation when the effect of this shift is statistically removed from Sahara $\Delta Z925$. The regression of Sahara $\Delta Z925$ on SHL latitude produces a slope of 5.1 ± 2.1 meters per degree latitude ($R=0.62$) in ERA-Interim, and when this dependence is removed to create a “latitude-detrended $\Delta Z925$ ”, this quantity has no statistically significant relationship with Sahel precipitation (Fig. 6c; the data that have not had the SHL shift removed are shown in Fig. 6b). Essentially, the statistically significant relationship between Sahel precipitation and many dynamical and thermodynamical quanti-

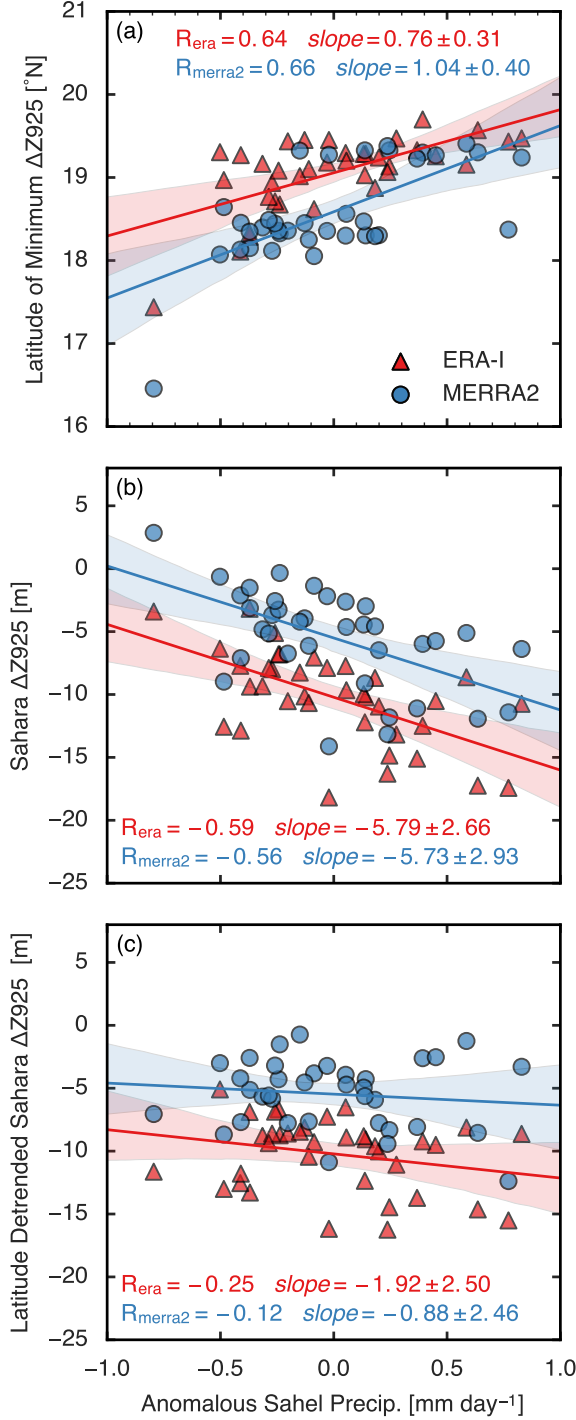


Figure 6: Regressions against Sahel precipitation (a) Heat low trough location (latitude of minimum 925 hPa ΔZ_{925}). (b) Sahara ΔZ_{925} (c) Sahara ΔZ_{925} with linear dependence on heat low trough location removed.

ties such as geopotential, divergence, and zonal wind is due to the meridional shift of the SHL circulation. When the linear dependence on SHL latitude of quantities shown in Fig. 4 and Fig. 7 is removed, significant first baroclinic mode geopotential changes remain over the Sahel and Sahara, but statistically significant shallow circulation changes are largely eliminated (not shown).

5 Vertical structure of changes in the SHL circulation

We now examine the vertical structure of interannual variations in the West African monsoon circulation, with focus on the Saharan overturning circulation. We first briefly revisit the poleward shift of the SHL during wet monsoon years, then discuss variations in the strength of the divergent component of the circulation.

The climatological low-level potential temperature is maximum around 22°N (Fig. 7a), poleward of the ITD. As Sahel precipitation increases, there is substantial cooling over the Sahel below 700 hPa, likely due to evaporative cooling of the land surface and reduced surface sensible heat fluxes into the boundary layer. Above 700 hPa, warming occurs poleward of 15°N into the midlatitudes. Potential temperature changes below 700 hPa over the Sahara are not statistically significant.

The ΔZ climatology (Fig. 7b) shows the near surface SHL centered around 18°N and the mid-tropospheric Saharan High centered around 25°N. The regression of ΔZ onto Sahel precipitation (Fig. 7b) shows that these structures expand or shift northward at every level. The cooling of the Sahel during wet years (Fig. 7a) is, by hydrostatic balance, accompanied by a thinning of the layer below 700 hPa and an anomalous low in the mid-troposphere (Fig. 7b). The cooling of the southern part of the SHL is accompanied by an increase in specific humidity (Fig. 7c) that is larger, in energy units, than the decrease in temperature, so that the low-level equivalent potential temperature, θ_e , is higher over the Sahel during wet years (Hurley and Boos, 2013). This enhanced low-level θ_e during

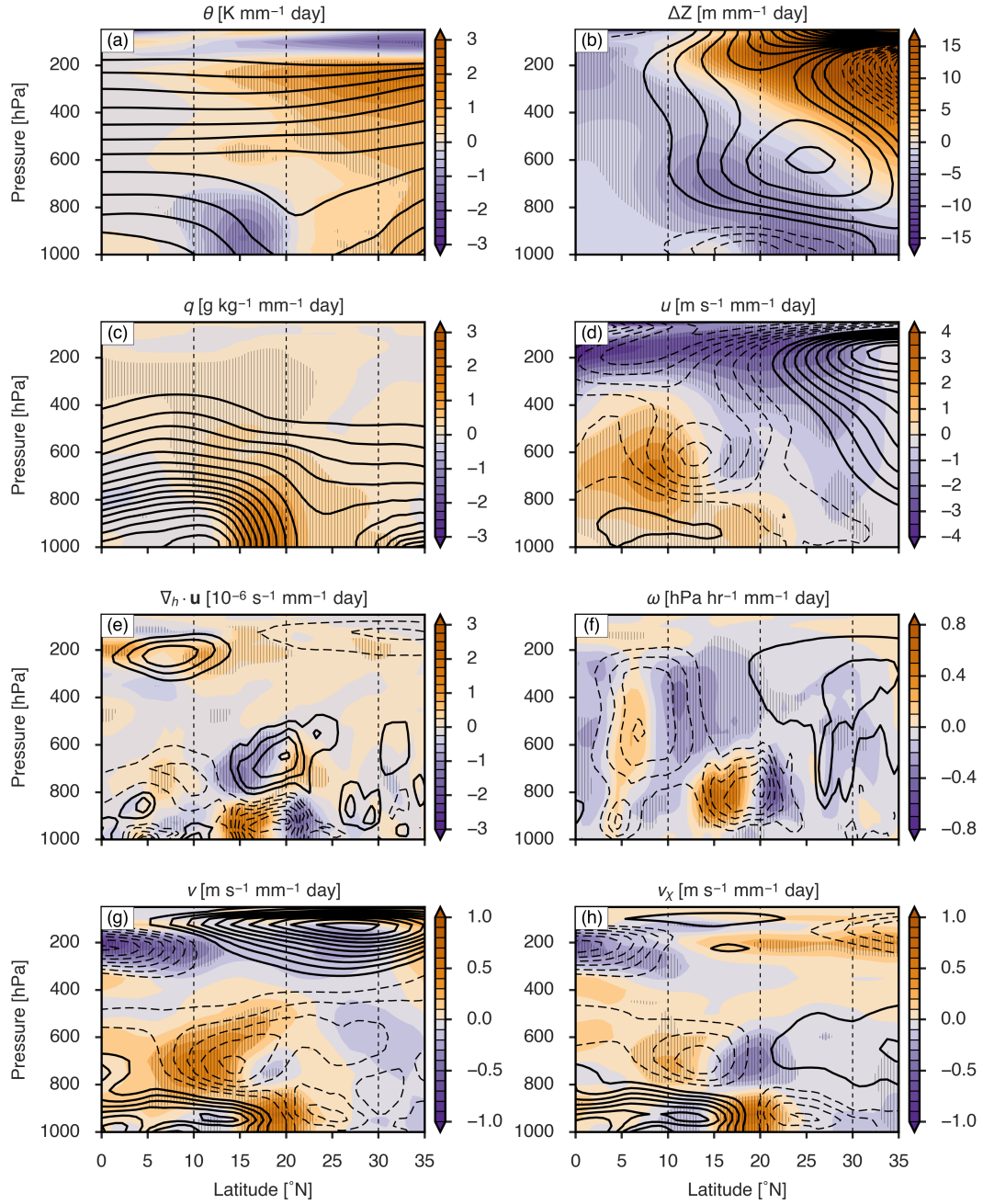


Figure 7: All panels show ERA-Interim zonal averages over 10°W–25°E. Colors indicate regression slope onto Sahel precipitation, hatching indicates statistical significance, and black contours indicate climatology (negative dashed, zero omitted). Units on regression slope imply per mm day⁻¹. (a) θ [K; contours every 5]. (b) ΔZ [meters; contours every 10]. (c) specific humidity [g kg⁻¹; contours every 1]. (d) u [m s⁻¹; contours every 2]. (e) Horizontal divergence [10^{-6} s⁻¹; contours every 1]. (f) ω [hPa hr⁻¹; contours every 0.5]. (g) v [m s⁻¹; contours every 0.5]. (h) v_χ [m s⁻¹; contours every 0.5].

wet years is accompanied by a warming throughout much of the middle and upper troposphere over the Sahel, as expected in convective quasi-equilibrium (Emanuel et al., 1994).

The zonal wind (Fig. 7d) closely describes the balanced component of the SHL circulation. During wet Sahel years, the near surface monsoon westerlies strengthen and expand into the region of the climatological ITD. The AEJ weakens and shifts poleward, in balance with the temperature and geopotential anomalies. The upper level tropical easterly jet expands poleward, modifying the northern hemisphere subtropical jet stream on its poleward boundary. These are all well known features of Sahel wet years, but no clear consensus exists on their causal relationship with Sahel rainfall variations (Nicholson, 2013).

The poleward shift in the divergent component of the SHL circulation, the Saharan overturning, can be seen as an anomalous, meridionally asymmetric quadrupole pattern in the anomalous divergence below 550 hPa (Fig. 7e; note the vertical dipole in the climatological mean fields centered at 20°N). There is also a meridional expansion of the upper tropospheric divergence associated with the monsoonal ITCZ. This upper tropospheric feature is also visible in the vertical velocity (Fig. 7f), with more deep ascent over the Sahel during wet years accompanying the anomalous dipole in low-level ascent that indicates a poleward shift in the Saharan overturning.

The meridional wind regression (Fig. 7g) shows an asymmetric quadrupole as well, with the southerly lobes of the quadrupole being spatially larger and of greater amplitude than the northerly lobes. However, this asymmetry in the anomalous meridional wind should not be interpreted as a weakening of the Saharan overturning circulation because we are considering a limited zonal mean, where the non-divergent component of meridional wind does not have to equal zero, unlike in the global zonal mean. When only the divergent component of the meridional wind is considered (Fig. 7h), the asymmetry in this quadrupole is substantially reduced. Nevertheless, there is meridional asymmetry in the quadrupole of anomalous divergence that is centered over the cli-

matological SHL (Fig. 7e), which would seem to indicate that the poleward shift of the SHL is accompanied by a weakening of the divergent component of the SHL circulation. Indeed, by mass continuity, the increased mass divergence in the upper troposphere that accompanies enhanced Sahel precipitation must be compensated by increased convergence at either at low or mid levels. In the next subsection we examine divergence vertically integrated over lower, middle and upper tropospheric layers to more precisely quantify variations in the divergent component of the SHL circulation.

6 Changes in layer-integrated divergence

The vertical section of divergence (Fig. 7d) allows identification of three layers that largely capture the changes in the divergent circulation: the lower troposphere (1000-800 hPa), the middle troposphere (800-550 hPa), and the upper troposphere (350-150 hPa). Taking a mass-weighted vertical integral of divergence over each layer (and over the remaining 550-350 hPa layer in which little divergence occurs) we see the climatological signatures of the divergent Hadley and SHL circulations (Fig. 8a). In the lower layer, the largest convergence is due to the shallow circulation which peaks near 20°N, but there is also some convergence in the ITCZ near 8°N. The middle troposphere exhibits large divergence at 20°N and substantial convergence at 10°N. Upper level divergence peaks around 8°N, the latitude of maximum precipitation and deep ascent, and the roughly equal magnitude and opposite signs of upper-tropospheric divergence and mid-tropospheric convergence at that latitude indicates that time-mean inflow to the deep, continental convergence zone occurs not near the surface but in the lower mid-troposphere. There is upper level convergence poleward of about 15°N, consistent with the northern Sahel and Sahara being regions of time-mean subsidence. Divergence in the 550–350 hPa layer is comparatively small, and divergence above 150 hPa is smaller still (not shown).

Regressing layer-integrated divergence onto Sahel precipitation (Fig. 8b) shows the now-familiar

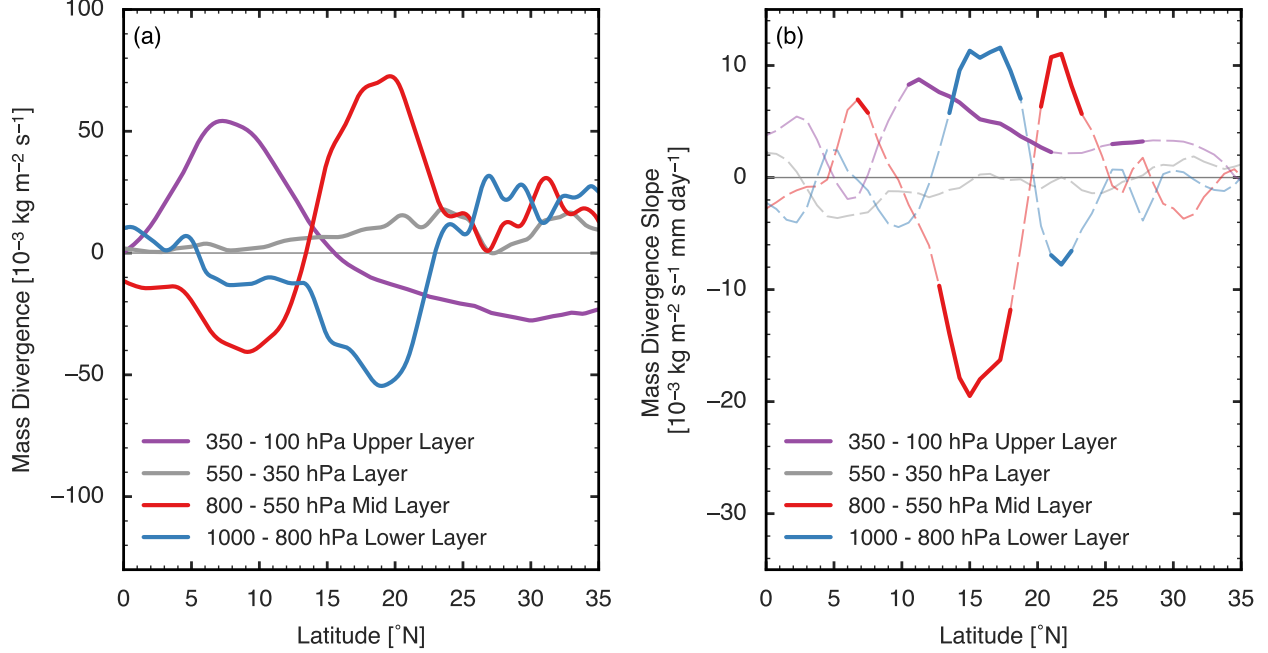


Figure 8: (a) Climatological vertical integrals of zonally averaged divergence over the specified layers, normalized for layer thickness (10^{-6} s^{-1}). (b) Regression slope of zonal and vertical averages of anomalous divergence over the specified layers ($10^{-6} \text{ s}^{-1} \text{ mm}^{-1} \text{ day}$). Statistically significant slopes are shown in dark, solid colors.

meridional dipole indicating a poleward shift of the climatological mean divergence field in the lower and mid layers, as well as a single-signed increase in upper-tropospheric divergence over the region. The asymmetry in the meridional shift is more clearly evident than in our previous depiction, with stronger changes on the equatorward lobe of the dipoles, implying that the Saharan overturning circulation weakens as it shifts poleward.

To assess the statistical robustness of this weakening of the Saharan overturning, we first note that the changes in divergence are almost entirely confined to the region between 10 $^{\circ}\text{N}$ and 25 $^{\circ}\text{N}$. So we horizontally average the layer-integrated divergences over 10 $^{\circ}\text{N}$ –25 $^{\circ}\text{N}$, 10 $^{\circ}\text{W}$ –25 $^{\circ}\text{E}$, thereby removing the antisymmetric component of the dipole and leaving a residual that corresponds to a net strengthening or weakening of divergence in each layer over the combined Sahel-Sahara region. There is some sensitivity to the meridional bounds used in this procedure, in particular the 10 $^{\circ}\text{N}$ bound. However, using an alter-

nate bound (such as 5 $^{\circ}\text{N}$) decreases the magnitude of the net divergence variations but does not qualitatively change the result.

The result of this area-averaging of the layer-integrated divergence shows that during wet Sahel years, upper-level divergence increases, mid-level divergence decreases, and low-level divergence increases (Fig. 9a). A strengthening of the Saharan overturning circulation would consist of a decrease in low-level divergence (enhanced convergence), and an increase in mid-level divergence; our area-averaged results have the opposite sign. Furthermore, Fig. 9b shows mid-level divergence is strongly anticorrelated with upper-level divergence, indicating that the enhanced upper-tropospheric divergence during wet monsoon years is balanced, in the time-mean column mass budget, by enhanced mid-tropospheric convergence. This balance is quantitatively confirmed by the fact that the regression coefficient relating upper- and mid-level layer-integrated convergence is approximately -1. Inter-

annual variations in the deep, precipitating monsoon circulation thus cannot be captured by a classic first-baroclinic mode that has maximum convergence near the surface and divergence at upper levels. Thorncroft et al. (2011) showed that the climatological mean moisture flux convergence in the Sahel has a complicated vertical structure with a weak maximum in our mid-tropospheric layer associated with flow in the Saharan overturning circulation, so it is perhaps not surprising that variations in the flow also do not have a simple classical structure. This issue is discussed further in the next section in the context of our idealized simulations.

7 Model of a weakening and shifting SHL circulation

Our idealized WRF model integrations, performed at 15 km horizontal resolution on a zonally periodic β -plane, are detailed in section 2 and in Shekhar and Boos (2016). A variety of surface albedo and SST forcings were applied individually about a control state to form an ensemble of model integrations. Instead of examining interannual variability within individual integrations, we look at the intra-ensemble variability of the long-term time-mean state and compare it to interannual variability within the re-analyses. Due to the zonally symmetric boundary conditions of the idealized model, the time-mean zonal wind is non-divergent and there are no large scale dynamical forcings such as those associated with ENSO or the South Asian monsoon, which could produce differences between observed interannual variability and the model intra-ensemble variability. Nevertheless, we find quantitative similarities in the statistical association between simulated monsoon precipitation and multiple dynamical variables.

The ensemble members are strongly forced (e.g. Saharan albedo changes of 0.1 to 0.2), so represent a wider range of ITCZ and SHL locations than is observed in the historical record. Fig. 10 shows how the mass streamfunction (obtained using the method of Döös and Nilsson, 2011) changes between integrations having the driest Sahel and those with the

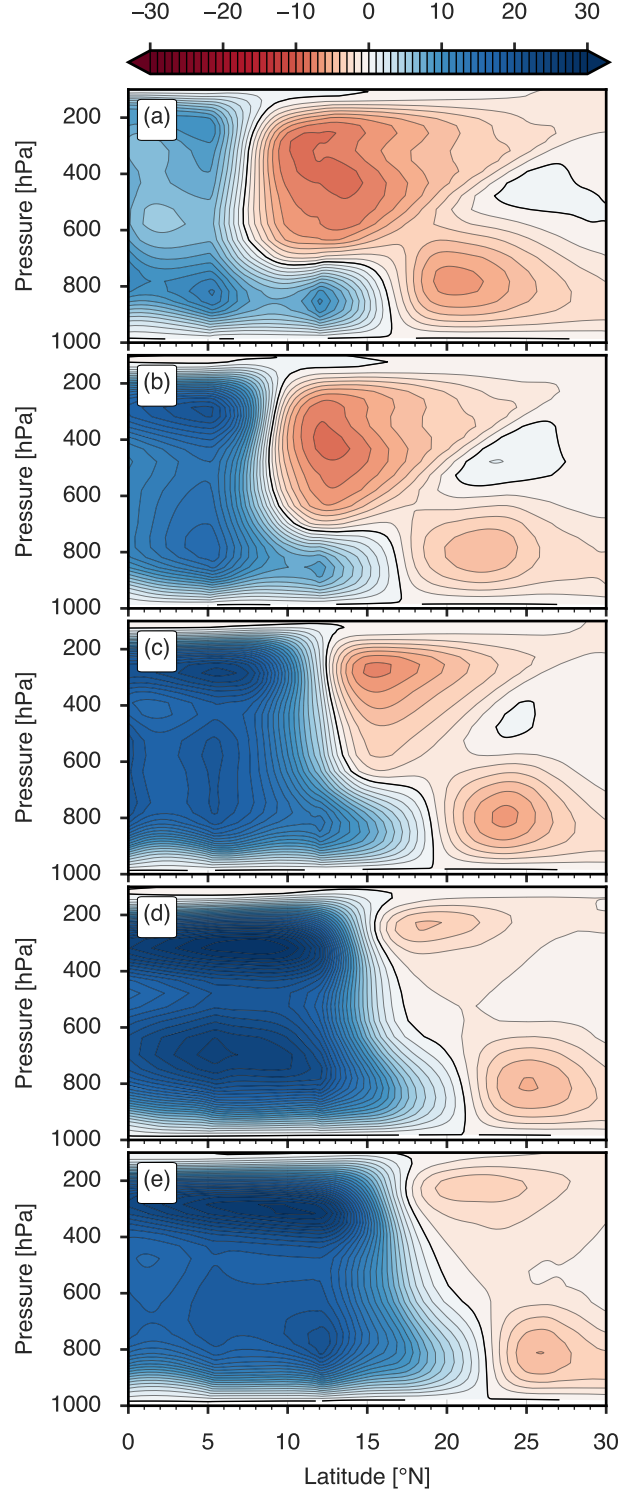


Figure 10: Mass streamfunctions (10^9 kg s^{-1}) ordered by increasing precipitation in the $10^\circ\text{--}20^\circ\text{N}$ box. (a) +2K SST forcing south of Africa. (b) Albedo increase of 0.10 over $12^\circ\text{--}32^\circ\text{N}$. (c) Control experiment. (d) -2K SST equatorial cold tongue, as in d. (e) Albedo decrease of 0.10 over $12^\circ\text{--}32^\circ\text{N}$.

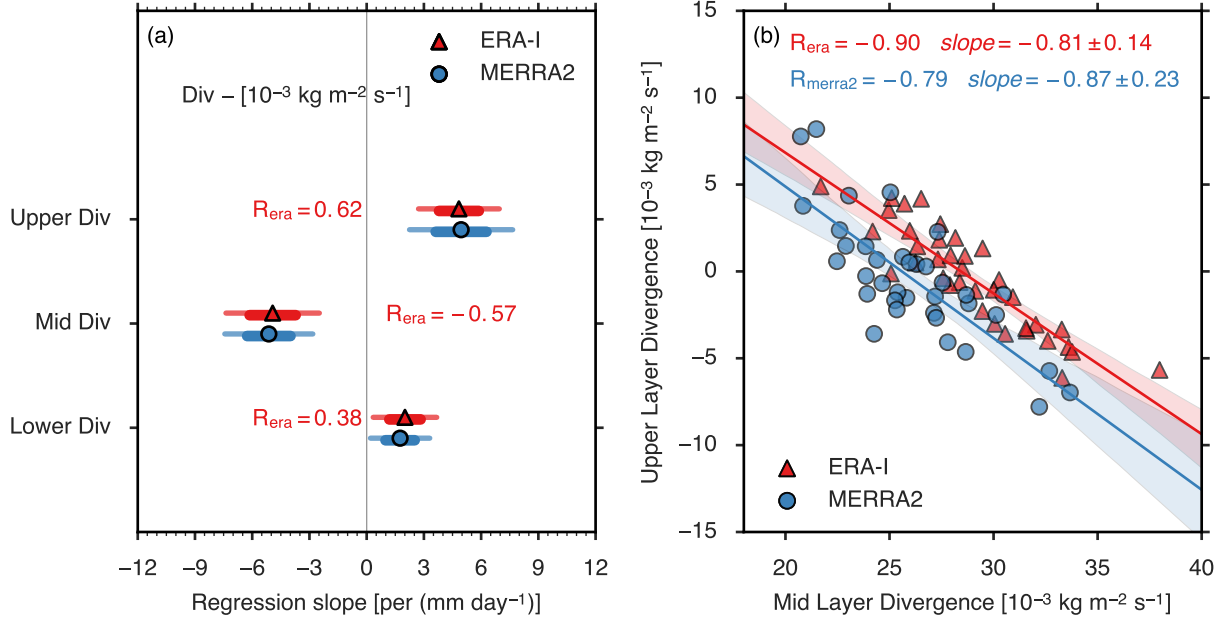


Figure 9: (a) 68% (thick) and 95% (thin) confidence intervals for the slope of the regression. Slopes shown for layer and area averaged divergence ($10^{-6} \text{ s}^{-1} \text{ mm}^{-1} \text{ day}$) regressed onto Sahel precipitation. (b) Regression of upper tropospheric divergence onto mid tropospheric divergence.

wettest Sahel (the model Sahel is also defined as the region $10\text{--}20^\circ\text{N}$). In the lowest precipitation state, deep ascent peaks at 8°N , and ascent in the SHL is well separated with a peak at 17°N . In this state, the summer Hadley cell is strong, the cross-equatorial winter Hadley cell is relatively weak, and the SHL circulation is relatively strong. As precipitation increases over the Sahel box (e.g. Fig. 10c), the ITCZ moves poleward into continent, the winter Hadley cell strengthens, the summer Hadley cell weakens, and the separation between the SHL ascent and the ITCZ decreases. As Sahel precipitation increases further (e.g. Fig. 10e), the winter Hadley cell continues to strengthen, the summer Hadley cell continues to weaken, and the shallow SHL ascent begins to merge with the ITCZ.

Quantitatively comparing our idealized model with observations is complicated by the task of choosing an appropriate region over which to average precipitation and divergence. In the reanalyses, the Sahel ($10^\circ\text{N--}20^\circ\text{N}$) always lies on the poleward edge of the ITCZ and the ascending branch of

the SHL circulation is centered in the region over which we averaged divergence ($10^\circ\text{N--}25^\circ\text{N}$). In the idealized model, the ITCZ and SHL move over a much wider latitude band, with the ITCZ centered south of the averaging region in some integrations and squarely within it in others (Fig. 10). Nevertheless, ascent in the model SHL always lies between 10°N and 25°N , so variations in the strength of mid-tropospheric divergence produced by the SHL circulation should be well captured by averages of the layer-integrated divergence between those latitude bounds. For this reason, we average precipitation and layer-integrated divergence over the same regions chosen for the reanalyses.

As expected, the observed interannual variability of both Sahel precipitation and SHL latitude is much smaller than variability in the model ensemble (Fig. 11a). There is rough quantitative agreement between the regression coefficients based on observed and simulated variables: the 95% confidence interval for the slope of model Sahel precipitation regressed on model SHL latitude overlaps with that of ERA-

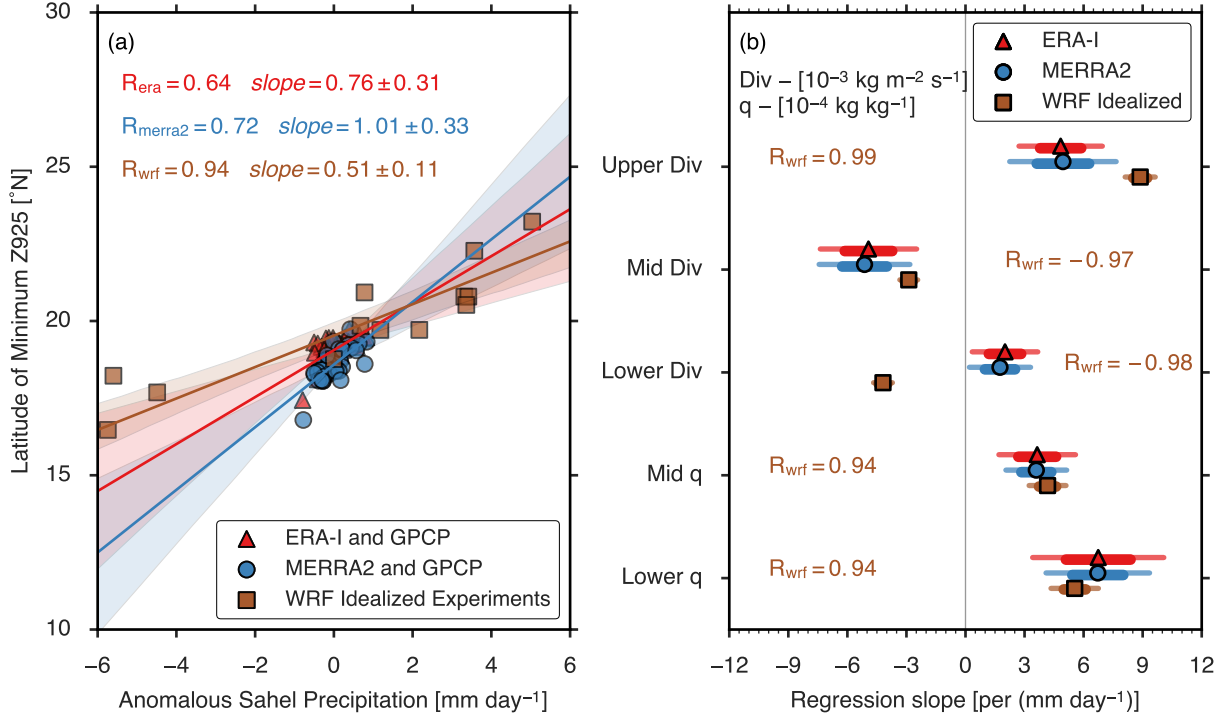


Figure 11: (a) Regression of the latitude of heat low location (minimum ΔZ_{925}) against precipitation. (b) 68% (thick) and 95% (thin) confidence intervals for regression slope. Slopes shown for layer and area averaged divergence ($10^{-6} \text{ s}^{-1} \text{ mm}^{-1} \text{ day}$) and specific humidity ($\text{g kg}^{-1} \text{ mm}^{-1} \text{ day}$) regressed onto Sahel precipitation. For the WRF data points, due to a different number of degrees of freedom (11), critical R values are 0.552, 0.683, and 0.800 at the 0.05, 0.01, and 0.001 significance levels.

Interim but does not overlap with the MERRA2 interval. The idealized model also exhibits associations between Sahel precipitation and upper-level divergence, mid-level convergence, and area-averaged, layer-integrated humidity that are quantitatively similar to those seen in observed interannual variability (Fig. 11b). This agreement is remarkable given that the model was not tuned to observed interannual variability: these simulations were performed for a different study (Shekhar and Boos, 2016) that was completed before this analysis was undertaken. However, the idealized model disagrees with observations in that it simulates enhanced low-level convergence when there is enhanced Sahel precipitation (recall that the reanalyses indicate a weak reduction of low-level convergence during anomalously rainy years). Enhanced precipitating ascent in the idealized model thus seems to be better described by a classic first-baroclinic mode vertical structure than in reanalyses. Whether this means that the model is unsuitable for representing interactions between the monsoonal ITCZ and the SHL circulation is unclear, in large part because there has been little study of the implications of deviations from a first-baroclinic mode structure for variability in monsoons.

Despite some bias in the vertical structure of the ITCZ, this idealized model clearly simulates a weakening and poleward shift of the Saharan overturning circulation in states with enhanced Sahel precipitation. Furthermore, the model results suggest that the circulation over West Africa exists on a continuum. At one end of the continuum, dry states have a coastal ITCZ close to the equator, large separation between the ITCZ and ascent in the SHL, and a strong Saharan overturning circulation with abundant mid-tropospheric divergence. At the other end of the continuum, the ITCZ is positioned much further poleward in a continental location, the winter Hadley cell is stronger while the summer Hadley cell is weaker, the overturning mass flux and mid-tropospheric divergence in the SHL circulation are weaker, and the ascending branches of the SHL and ITCZ have begun to merge to produce a vertical structure closer to that of first-baroclinic mode ascent common in deep convective regions..

8 Discussion

Previous work has found intriguing associations between Sahel precipitation and the SHL, but the mechanism responsible for these associations has remained unclear. A close reading of previous literature reveals contradictory results concerning even the sign of the association, with some arguing that a stronger SHL causes increased Sahel precipitation (e.g Haarsma et al., 2005; Biasutti et al., 2009; Lavaysse et al., 2009, 2010a) while others argue that a stronger SHL circulation weakens Sahel precipitation (Peyrill   and Lafore, 2007) or at least is correlated with weaker Sahel precipitation (Lavaysse et al., 2010b). Previous studies have not used a consistent definition for the term ‘‘Saharan Heat Low’’, which complicates comparison of prior results.

This study shows that the association of the SHL with Sahel precipitation is best described as a poleward shift and weakening of the SHL circulation during wet Sahel years. We showed that 925 hPa geopotential height over the Sahara was negatively correlated with Sahel precipitation, quantitatively reproducing the results of Biasutti et al. (2009). However, the decrease in geopotential was located north of the climatological mean geopotential minimum, suggesting a northward expansion or shift, rather than an intensification, of the low-level trough during wet monsoon years. Changes in the thickness of the lower troposphere had a meridional dipole structure centered on the zonally elongated climatological maximum in thickness, which is also indicative of a poleward shift in the heat low. When the linear relationship of 925 hPa geopotential with the latitude of the heat low was statistically removed, no statistically significant relationship remained between Sahel precipitation and Saharan 925 hPa geopotential height.

Weakening of the SHL circulation was best seen through examination of the divergent component of the flow. Upper tropospheric divergence over the Sahel increased during wet years, as expected for a deep, precipitating monsoon circulation. Shallow ascent in the Saharan overturning circulation shifted poleward and weakened during wet years, as ev-

identified by the meridionally asymmetric dipole of anomalous vertical velocity in the lower troposphere over the Sahara (Fig. 7f). Asymmetric meridional dipoles were also seen in the divergence integrated over the lower and middle troposphere, confirming this weakening and poleward shifting of the shallow circulation. The increased upper-level divergence during wet years is balanced, in the column integrated mass budget, by increased convergence in the lower mid-troposphere, indicating some departure from classic first-baroclinic mode structures that have maximum convergence near the surface. Nevertheless, these results suggest a trade-off between the shallow and deep modes of vertical ascent, where unusually wet years exhibit a strong deep circulation and weak shallow SHL circulation.

An idealized model of West Africa was used to produce an ensemble of integrations forced by applied SST and land surface albedo anomalies. This ensemble explores a variety of climatic states with a much greater range than that of interannual variations in reanalyses. Nevertheless, without any tuning, the intra-ensemble variability of the idealized model climatological means exhibits a similar relationship between the Saharan overturning circulation and Sahel precipitation seen in observed interannual variability. Increases in deep, precipitating ascent in the model were better described by a classic first-baroclinic mode than they were in reanalyses, but both the model and the reanalyses clearly showed a weakening of mid-tropospheric divergence in the SHL circulation as monsoon precipitation increased. This is consistent with the results of Peyrillé and Lafore (2007), who showed that dry and warm outflow from the Saharan high weakened Sahel precipitation in another idealized model. Our observational results disprove the hypothesis that increased Sahel precipitation is caused by a strengthening of shallow divergent flow in the SHL circulation. To be clear, the underlying cause of changes in the idealized model was anomalies in SST and land surface albedo, but variations in the SHL circulation could be part of the mechanism by which those forcings influence Sahel precipitation.

One major caveat is worth noting. Fig. 2c showed

that interannual variations in GPCP precipitation exhibit a “monopole” pattern over West Africa since 1979. The reanalysis precipitation fields in ERA-Interim and MERRA-2 show more of a dipole pattern of interannual variability over this period, with a statistically significant decrease in precipitation over the Gulf of Guinea (5–10°N) during wet Sahel years (not shown). This dipole pattern of precipitation anomalies, which is consistent with a meridional shift of the ITCZ and which characterized rainfall variations earlier in the twentieth century (Losada et al., 2012), has not been seen in precipitation measurements after the 1970s. So it seems possible that the reanalyses are representing a biased spatial pattern of precipitation variability during the past few decades, assuming the precipitation observations are not themselves in error. This uncertainty in precipitation over the coastal Gulf of Guinea region influenced our decision to use 10°N as the southern boundary when calculating area averaged, layer integrated divergence, so that this uncertain region is excluded. Even if the reanalyses have substantial error in their representation of interannual variability over this region, it seems unlikely that this error would compromise the qualitative nature of our results (e.g. change the sign of correlations between Sahel precipitation and geopotential height, divergence, and ascent over the Sahara in two reanalysis products). Confirmation of some of these associations in an idealized model lends further confidence in our results. Nevertheless, it is good to bear in mind that reanalyses have bias, even while they remain a useful tool for understanding historical atmospheric variability over the last few decades.

Important questions remain. Does the association between a weak Saharan overturning circulation and increased Sahel rainfall also hold on intraseasonal or synoptic time scales? Lavaysse et al. (2010a), Lavaysse et al. (2010b), and Evan et al. (2015) examine certain features of the SHL circulation on these timescales and provide evidence for relationships of both signs. More fundamentally, what mechanism causes Sahel precipitation to weaken while the SHL circulation strengthens? Peyrillé and Lafore (2007) provide evidence from an idealized two-dimensional

model that Sahel rainfall can be weakened by warm and dry mid-tropospheric outflow in the SHL circulation. Another possibility is that the deep, precipitating circulation and the shallow SHL circulation are both responding independently to some external forcing. Further work is required to determine which mechanism operates in reality and whether it is relevant to variability in other monsoon regions.

Acknowledgments

Both authors were supported by National Science Foundation grant AGS-1253222. This work was supported in part by the facilities and staff of the Yale University Faculty of Arts and Sciences High Performance Computing Center. Computing support was also provided by Yellowstone (ark:/85065/d7wd3xhc), supported by NCAR's Computational and Information Systems Laboratory. We would also like to thank Xavier Levine for many fruitful discussions.

References

- Adler, R. F., and Coauthors, 2003: The Version-2 Global Precipitation Climatology Project (GPCP) Monthly Precipitation Analysis (1979 - Present). *Journal of Hydrometeorology*, **4** (6), 1147–1167, doi:10.1175/1525-7541(2003)004<1147:TVGPCP>2.0.CO;2.
- Biasutti, M., A. H. Sobel, and S. J. Camargo, 2009: The Role of the Sahara Low in Summertime Sahel Rainfall Variability and Change in the CMIP3 Models. *Journal of Climate*, **22** (21), 5755–5771, doi:10.1175/2009JCLI2969.1.
- Botvinnik, O., and Coauthors, 2016: seaborn: v0.7.0 (January 2016). URL <https://github.com/mwaskom/seaborn>, doi:10.5281/zenodo.45133.
- Charney, J., P. H. Stone, and W. J. Quirk, 1975: Drought in the Sahara: A Biogeophysical Feedback Mechanism. *Science*, **187** (4175), 434–435, doi:10.1126/science.187.4175.434.
- Dee, D. P., and Coauthors, 2011: The ERA-Interim reanalysis: Configuration and performance of the data assimilation system. *Quarterly Journal of the Royal Meteorological Society*, **137** (656), 553–597, doi:10.1002/qj.828.
- Derbyshire, S., I. Beau, P. Bechtold, J.-Y. Grandpeix, J.-M. Piriou, J.-L. Redelsperger, and P. Soares, 2004: Sensitivity of moist convection to environmental humidity. *Quarterly Journal of the Royal Meteorological Society*, **130** (604), 3055–3079, doi:10.1256/qj.03.130.
- Dezfuli, A. K., and S. E. Nicholson, 2011: A note on long-term variations of the African easterly jet. *International Journal of Climatology*, **31** (13), 2049–2054, doi:10.1002/joc.2209.
- Döös, K., and J. Nilsson, 2011: Analysis of the Meridional Energy Transport by Atmospheric Overturning Circulations. *Journal of the Atmospheric Sciences*, **68** (8), 1806–1820, doi:10.1175/2010JAS3493.1.
- Eltahir, E. a. B., and C. Gong, 1996: Dynamics of wet and dry years in West Africa. *Journal of Climate*, **9** (5), 1030–1042, doi:10.1175/1520-0442(1996)009<1030:DOWADY>2.0.CO;2.
- Emanuel, K. A., J. David Neelin, and C. S. Bretherton, 1994: On large-scale circulations in convecting atmospheres. *Quarterly Journal of the Royal Meteorological Society*, **120** (519), 1111–1143, doi:10.1002/qj.49712051902.
- Evan, A. T., C. Flamant, C. Lavaysse, C. Kocha, and A. Saci, 2015: Water Vapor Forced Greenhouse Warming over the Sahara Desert and the Recent Recovery from the Sahelian Drought. *Journal of Climate*, **28**, 108–123, doi:10.1175/JCLI-D-14-00039.1.
- Folland, C. K., T. N. Palmer, and D. E. Parker, 1986: Sahel rainfall and worldwide sea temperatures, 1901–85. *Nature*, **320** (6063), 602–607, doi:10.1038/320602a0.
- Gelaro, R. and co-authors, 2016 in preparation: MERRA-2 Overview. *Journal of Climate*.

- Giannini, A., R. Saravanan, and P. Chang, 2003: Oceanic forcing of Sahel rainfall on interannual to interdecadal time scales. *Science*, **302** (5647), 1027–30, doi:10.1126/science.1089357.
- Grist, J. P., and S. E. Nicholson, 2001: A Study of the Dynamic Factors Influencing the Rainfall Variability in the West African Sahel. *Journal of Climate*, **14** (7), 1337–1359.
- Haarsma, R. J., F. M. Selten, S. L. Weber, and M. Kliphuis, 2005: Sahel rainfall variability and response to greenhouse warming. *Geophysical Research Letters*, **32** (1), 17 702, doi:10.1029/2005GL023232.
- Hagos, S. M., and K. H. Cook, 2007: Dynamics of the West African monsoon jump. *Journal of Climate*, **20** (21), 5264–5284, doi:10.1175/2007JCLI1533.1.
- Holloway, C., and J. D. Neelin, 2009: Moisture vertical structure, column water vapor, and tropical deep convection. *Journal of the Atmospheric Sciences*, doi:10.1175/2008JAS2806.1.
- Hsieh, J.-S., and K. H. Cook, 2005: Generation of African Easterly Wave Disturbances: Relationship to the African Easterly Jet. *Monthly Weather Review*, **133** (5), 1311–1327, doi:10.1175/MWR2916.1.
- Hurley, J. V., and W. R. Boos, 2013: Interannual Variability of Monsoon Precipitation and Local Subcloud Equivalent Potential Temperature. *Journal of Climate*, **26**, 9507–9527, doi:10.1175/JCLI-D-12-00229.1.
- Lavaysse, C., C. Flamant, and S. Janicot, 2010a: Regional-scale convection patterns during strong and weak phases of the Saharan heat low. *Atmospheric Science Letters*, **11** (4), 255–264.
- Lavaysse, C., C. Flamant, S. Janicot, and P. Knipfertz, 2010b: Links between African easterly waves, midlatitude circulation and intraseasonal pulsations of the West African heat low. *Quarterly Journal of the Royal Meteorological Society*, **136** (1), 141–158, doi:10.1002/qj.555.
- Lavaysse, C., C. Flamant, S. Janicot, D. J. Parker, J. P. Lafore, B. Sultan, and J. Pelon, 2009: Seasonal evolution of the West African heat low: A climatological perspective. *Climate Dynamics*, **33** (2-3), 313–330, doi:10.1007/s00382-009-0553-4.
- Losada, T., B. Rodriguez-Fonseca, E. Mohino, J. Bader, S. Janicot, and C. R. Mechoso, 2012: Tropical SST and Sahel rainfall: A non-stationary relationship. *Geophysical Research Letters*, **39** (12), 1–7, doi:10.1029/2012GL052423.
- Neelin, J. D., and N. Zeng, 2000: A Quasi-Equilibrium Tropical Circulation Model{–}Formulation*. *Journal of the Atmospheric Sciences*, **57** (11), 1741–1766, doi:10.1175/1520-0469(2000)057<1741:AQETCM>2.0.CO;2.
- Nicholson, S., 2005: On the question of the recovery of the rains in the West African Sahel. *Journal of Arid Environments*, **63** (3), 615–641, doi:10.1016/j.jaridenv.2005.03.004.
- Nicholson, S., and J. Grist, 2001: A conceptual model for understanding rainfall variability in the West African Sahel on interannual and interdecadal timescales. *International Journal of Climatology*, **21** (14), 1733–1757, doi:10.1002/joc.648.
- Nicholson, S. E., 2013: The West African Sahel: A Review of Recent Studies on the Rainfall Regime and Its Interannual Variability. *ISRN Meteorology*, **2013** (4), 1–32, doi:10.1155/2013/453521.
- Nicholson, S. E., A. K. Dezfuli, and D. Klotter, 2011: A Two-Century Precipitation Data Set for the Continent of Africa. *Bulletin of the American Meteorological Society*, doi:10.1175/BAMS-D-11-00212.1.
- Nie, J., W. R. Boos, and Z. Kuang, 2010: Observational Evaluation of a Convective Quasi-Equilibrium View of Monsoons. *Journal of Climate*, **23** (16), 4416–4428, doi:10.1175/2010JCLI3505.1.

- Peyrillé, P., and J.-P. Lafore, 2007: An Idealized Two-Dimensional Framework to Study the West African Monsoon. Part II: Large-Scale Advection and the Diurnal Cycle. *Journal of the Atmospheric Sciences*, **64** (8), 2783–2803, doi:10.1175/JAS4052.1.
- Peyrillé, P., J.-P. Lafore, and A. Boone, 2016: The annual cycle of the West African monsoon in a two-dimensional model: mechanisms of the rain-band migration. *Quarterly Journal of the Royal Meteorological Society*, **142** (696), 1473–1489, doi:10.1002/qj.2750.
- Peyrillé, P., J.-P. Lafore, and J.-L. Redelsperger, 2007: An Idealized Two-Dimensional Framework to Study the West African Monsoon. Part I: Validation and Key Controlling Factors. *Journal of the Atmospheric Sciences*, **64** (8), 2765–2782, doi:10.1175/JAS3919.1.
- Rácz, Z., and R. K. Smith, 1999: The dynamics of heat lows. *Quarterly Journal of the Royal Meteorological Society*, **125** (553), 225–252, doi:10.1002/qj.49712555313.
- Rousseeuw, P. J., and A. M. Leroy, 2005: *Robust regression and outlier detection*, Vol. 589. John Wiley & Sons.
- Schneider, T., T. Bischoff, and G. H. Haug, 2014: Migrations and dynamics of the intertropical convergence zone. *Nature*, **513** (7516), 45–53, doi:10.1038/nature13636.
- Seabold, J., and J. Perktold, 2010: Statsmodels: Econometric and statistical modeling with python. *Proceedings of the 9th Python in Science Conference*.
- Shekhar, R., and W. R. Boos, 2016: Improving Energy-Based Estimates of Monsoon Location in the Presence of Proximal Deserts. *Journal of Climate*, **29** (13), 4741–4761, doi:10.1175/JCLI-D-15-0747.1.
- Skamarock, W. C., and Coauthors, 2008: A description of the advanced research WRF version 3. *NCAR technical note*.
- Sobel, A. H., and T. Schneider, 2009: Single-layer axisymmetric model for a Hadley circulation with parameterized eddy momentum forcing. *Journal of Advances in Modeling Earth Systems*, **2**, 10.
- Thorncroft, C. D., and M. Blackburn, 1999: Maintenance of the African easterly jet. *Quarterly Journal of the Royal Meteorological Society*, **125** (555), 763–786, doi:10.1002/qj.49712555502.
- Thorncroft, C. D., H. Nguyen, C. Zhang, and P. Peyrillé, 2011: Annual cycle of the West African monsoon: regional circulations and associated water vapour transport. *Quarterly Journal of the Royal Meteorological Society*, **137** (654), 129–147, doi:10.1002/qj.728.
- U.K. Met Office, 2015: *Iris: A Python library for analysing and visualising meteorological and oceanographic data sets*. Exeter, Devon, v1.8 ed., URL <http://scitools.org.uk/>.
- Vizy, E. K., and K. H. Cook, 2009: A mechanism for African monsoon breaks: Mediterranean cold air surges. *Journal of Geophysical Research: Atmospheres*, **114** (1), 1–19, doi:10.1029/2008JD010654.
- Zhang, C., D. S. Nolan, C. D. Thorncroft, and H. Nguyen, 2008: Shallow Meridional Circulations in the Tropical Atmosphere. *Journal of Climate*, **21** (14), 3453–3470, doi:10.1175/2007JCLI1870.1.